Modeling water transport properties in carbon nanotubes: Interplay between force-field flexibility and geometrical parameters

Luana S. Moreira, Douglas D. de Vargas, and Mateus H. Köhler*
Departamento de Física, Universidade Federal de Santa Maria, 97105-900 Santa Maria, Brazil

(Received 30 November 2022; accepted 29 August 2023; published 19 September 2023)

Modeling water and other liquids in computational simulations requires a large set of parameters. Many works have been devoted to finding new, improved water models, with almost all of them designed for bulk systems. Here, we use carbon nanotubes as a play model to investigate the effects of introducing flexibility in water force fields during molecular dynamics simulations of nanoconfined water. We explore six different models to show that viscosity, diffusion, and dipole orientation are vastly influenced by the flexibility and the family of force fields used. Particularly, we found the level of confinement (decreasing the nanotube's diameter) to increase discrepancies in the description of the dipole alignment. In smaller (10,10) nanotubes, the flexible version of the transferable intermolecular potential with three points (TIP3P/Fs) features a high directionality, while its rigid counterpart shows a more distributed dipole orientation. Both viscosity and diffusion are also extremely dependent on the force-field family, with the flexible version of the simple point charge (SPC/Fw) featuring the lower confidence interval.

DOI: 10.1103/PhysRevE.108.034116

I. INTRODUCTION

Carbon nanotube (CNT) membranes are known for exhibiting higher water flux with lower energy than current membranes. The possibility to filter out particles that are too small for conventional purification systems puts CNT-based membranes in the spotlight for a new generation of green, sustainable materials. Several studies have shown that these highly appreciated mechanisms are closely related to the superficial water interactions at the solid-liquid interface in CNTs [1]. The full extent to which we can use these systems will depend on our ability to explore and predict the physical and chemical properties driving water transport in such exciting environments.

In recent decades, several experimental efforts have been made to elucidate the water transport inside CNTs. The highly reduced geometries, timescales, and other difficulties associated with nanoscale heterogeneity have made this task far too challenging. From the grand canonical Monte Carlo (GCMC) simulations of Maddox and Gubbins [2], to the molecular dynamics (MD) study by Hummer *et al.* [3] and the experimental work by Naguib *et al.* [4], many works have been devoted to fully comprehending the water-filling phenomenon of CNTs. Remarkably, we can refer to more recent works by Secchi *et al.* [5], tracing water molecules emerging from individual nanotubes, and by Hassan *et al.* [6], using two-dimensional nuclear magnetic resonance (NMR) diffusion relaxation to show how heterogeneous water diffusion is inside CNTs.

Classical MD simulations have often been applied to assess a plethora of new data regarding the water dynamics and structure inside nanopores such as CNTs. In the last two decades, we have advanced our understanding of the mechanisms underlying the superflux of water in CNTs [7], the heterogeneity in diffusion [8], the breakdown of classical hydrodynamic theory at nanoscale [9], and so many other phenomena where MD simulations have contributed to clarifying the physical and chemical processes taking place.

These simulations normally employ water force fields that are actually designed to predict bulk's water properties. However, water confined at the nanoscale presents exciting, new behaviors that can affect our capacity to properly model it. When modeling water in a MD simulation, we use a set of parameters to describe their bond length, angles, and van der Waals (vdW) and Coulomb interaction parameters. Additionally, we can introduce several degrees of freedom (e.g., bond stretching, angle bending, variations in charge distribution), allowing the water force field to be either flexible or polarizable. Even among rigid force fields, there are remarkable differences, such as in the number and location of the charge sites. It is important to note that even at the bulk phase, it remains a challenge to find a model that accurately reproduces all of the experimental properties of water simultaneously [10]. It becomes an important choice, and this choice depends on the information one wants to collect from the simulation.

Here we use six different force fields to model water dynamics inside CNTs to show that the choice between different parameters can impact the prediction of transport behavior. Three of the models are rigid simple point charge (SPC/E), transferable intermolecular potential with three points (TIP3P), and with four points (TIP4P/2005) and the others are flexible (SPC/Fw, TIP3P/Fs, and TIP4P/2005f). We found different confidence intervals (CIs) when calculating both water viscosity and diffusion inside CNTs with different lengths. Interestingly, the flexible SPC/Fw presents higher oscillations in the autocorrelation function (ACF) calculations, but shows the smaller CI in the viscosity and diffusion results among all the investigated models. Remarkably, we found a radius-dependent dipole alignment in the

*mateus.kohler@ufsm.br

TABLE I. LJ parameters and charge details of each force field.

	SPC/E [13]	SPC/Fw [14]	TIP3P [15]	TIP3P/Fs [16]	TIP4P/2005 [17]	TIP4P/2005f [18]
Flexible?	No	Yes	No	Yes	No	Yes
ε_{OO} (kcal/mol)	0.15535	0.155425	0.1521	0.1522	0.185207	0.185207
σ_{OO} (Å)	3.166	3.165492	3.15061	3.1506	3.1589	3.1644
q_H (e)	0.4238	0.41	0.417	0.417	0.5564	0.5564
d_{OM} (Å)					0.1546	0.15555
d_{OH} (Å)	1.0	1.012	0.9572	0.96	0.9572	0.9419
θ_{HOH} (deg)	109.4667	113.24	104.52	104.5	104.52	107.4
K_b (kcal/mol Å^2)	∞	529.581	∞	529.581	∞	540.764
K_θ (kcal/mol rad^2)	∞	37.95	∞	34.0435	∞	87.90

interfacial water for all models, with the flexible TIP3P/Fs exhibiting an anomalous directional dipole orientation in smaller nanotubes.

II. COMPUTATIONAL DETAILS AND METHODS

A. Modeling water and nanotubes

MD simulations of water confined in CNTs were performed using the LAMMPS package [11]. Initially, we considered (10,10) CNTs with lengths ranging between 20, 40, 80, and 160 nm in order to evaluate the impact of the system's size and number of particles over the water properties prediction. Following this, we varied the radius of the nanotube to investigate the existence of a radius dependence on the transport properties of the different water models.

The interaction potential is given by Lennard-Jones (LJ) and Coulomb terms, namely,

$$U_{\alpha\beta}(r) = 4\epsilon_{\alpha\beta}\left[\left(\frac{\sigma_{\alpha\beta}}{r}\right)^{12} - \left(\frac{\sigma_{\alpha\beta}}{r}\right)^{6}\right] + \frac{1}{4\pi\epsilon_0}\frac{q_\alpha q_\beta}{r}, \quad (1)$$

where α and β stand for different atomic species (i.e., oxygen, hydrogen, and carbon). In the four-point force fields (TIP4P/2005 and TIP4P/2005f), water is modeled as masses at the oxygen and hydrogen sites, where positive charges are placed in the H atoms and the negative charge is placed in a fictitious site M along the bisector of the HOH angle (θ_{HOH}), coplanar with O and H atoms. We used $\varepsilon_{CC} = 0.123$ kcal/mol and $\sigma_{CC} = 0.326$ nm to model the carbon LJ interaction parameters. LJ parameters and other details for each water model are shown in Table I. Lorentz-Berthelot mixing rules were employed for the nonbonded interactions. Long-range electrostatic interactions were calculated by the particle-particle particle-mesh method, and the LJ cutoff distance was set to 1 nm. The SHAKE algorithm [12] was used to keep the water molecules rigid, while specific harmonic parameters were implemented to describe bond stretching, $K_b(r - r_0)^2$, and angle bending, $K_\theta(\theta - \theta_0)^2$, in the flexible force fields.

B. Simulation details

The simulations were conducted in the canonical NVT ensemble with temperature T set to 300 K by a Nosé-Hoover thermostat [19]. The initial geometry and number of particles were based on previous works [9,20], where an *effective density* $\rho_{eff} = 0.88$ g/cm^3 is achieved after the previously empty cavity of CNT is invaded with water from two reservoirs at 0.99 g/cm^3, both at ambient conditions of pressure (1 bar) and temperature (300 K). The number of water molecules and nanotube details are given in Table II. Periodic boundary conditions were applied in the axial direction of the tubes, which results in isolated infinite nanotubes. In order to keep things as simple as possible, the positions of the carbon atoms were fixed, i.e., not integrated during the simulations. The system was equilibrated for 10 ns with the time step set to 1 fs. Finally, simulations of 10 ns of data accumulation were performed.

We analyzed the diffusion mechanism of water by the scaling behavior between the mean squared displacement (MSD) and time,

$$\langle|\vec{r}(t) - \vec{r}(0)|^2\rangle = ADt^n, \quad (2)$$

where the angular brackets denote an average over time origins and all water molecules, $\vec{r}(t)$ is the displacement of a molecule during the time interval t, A is a constant that assumes values twice the dimensionality of the system (2, 4, or 6), and D stands for the diffusion coefficient. The n exponent refers to the diffusion regime: $n = 1$ for the linear Fickian diffusion, $n > 1$ for superdiffusive regime, and $n < 1$ for subdiffusive regime. Since the nanopore confinement in the x and y directions hinders the molecules' radial displacement, we only considered the axial diffusion D_z ($A = 2$).

For the viscosity calculations, we used the Green-Kubo (GK) relations [21],

$$\eta = \frac{V}{k_B T}\int_0^\infty dt\langle P_{\alpha\beta}(t)P_{\alpha\beta}(0)\rangle,$$
$$P_{\alpha\beta} = \frac{1}{V}\left(\sum_{i=1}^{N}\frac{p_{i\alpha}p_{i\beta}}{m} + \sum_{i=1}^{N}\sum_{j>i}^{N} r_{ij\alpha}f_{ij\beta}\right), \quad (3)$$

TABLE II. Length (l_z) and the respective average amount of water molecules inside the (10,10) nanotube.

l_z (nm)	H_2O
20	500
40	1000
80	2000
160	4000

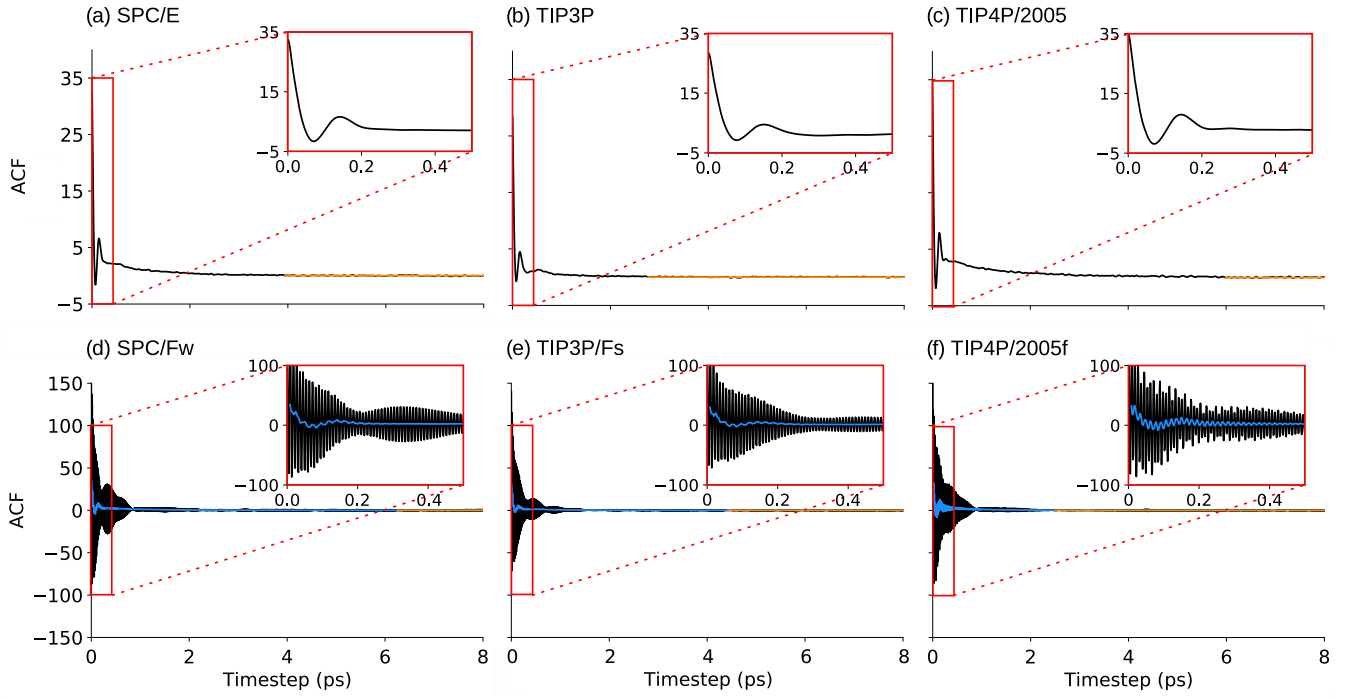

FIG. 1. Normalized autocorrelation functions for rigid and flexible water models inside (10,10) CNTs. We highlight (orange) the plateau region (at the end of each curve) and, for the flexible models in (b), (d), and (f), we also plot (blue) their moving average.

where $P_{\alpha\beta}$ is the stress tensor, $r_{ij} = |\vec{r}_i - \vec{r}_j|$, $f_{ij} = -\partial U(r_{ij})/\partial r_{ij}$, and $\alpha, \beta \in (x, y, z)$ denotes Cartesian components. The stress tensor can be calculated as inside the force calculation subroutine. In this work, the axial component (P_{xy}) was averaged to describe the viscosity of the fluids inside the nanopores [9]. We have collected the stress tensor components at each time step in order to ensure maximum accuracy with the upper limit of 50 ps. Following this, the converged autocorrelation functions (ACF) were integrated, as shown in Fig. 1. Three sets of simulations with different initial thermal velocity distributions were averaged to build the ACF and MSD curves.

We used the confidence interval (CI), with a 95% confidence level, to estimate the uncertainty as the properties are averaged. A CI is a range of estimates for a particular parameter in a sample: A larger sample would produce a narrower CI and a greater variability produces a wider CI. The CI is obtained through a Student's probability density function (t) with $n-1$ degrees of freedom as

$$\left(\bar{x} - t_{n-1}\frac{s}{\sqrt{n}} \quad , \quad \bar{x} + t_{n-1}\frac{s}{\sqrt{n}}\right), \tag{4}$$

where the right and left sides represent the upper and the lower limits, respectively, $\bar{x}$ is the sample average, n stands for the number of samples, and s is the sample standard deviation.

III. RESULTS AND DISCUSSION

A. Shear viscosity

In the GK method, the main contribution to the viscosity calculation comes from the tail of the stress tensor ACF. We show, in Fig. 1, the normalized ACFs of the nondiagonal components of the pressure tensor for confined water at 300 K. For the rigid models, in Figs. 1(a)–1(c), we notice two decay regimes (both monotonically), i.e., one for short times (fast scale) and another for higher times (slow scale of time). The first is sharply decaying (faster than $1/t$), while the second decreases smoothly with time. This is in stark contrast to the flexible models, in Figs. 1(d)–1(f), where we can notice higher oscillatory regimes. They can also be divided into fast and slow decay regimes. However, it is clearly taking a longer time for the ACFs associated with flexible force fields to reach convergence. This behavior will, in turn, lead to several consequences related to the viscosity determination, as will be discussed throughout the paper.

In order to eliminate some of the data randomness, leaving a smooth trend as a rigidlike ACF, a moving average was applied to the flexible models' ACFs, as shown by the blue lines in Figs. 1(d)–1(f). The estimated trend $\hat{T}$ of the time series y_t can be written as

$$\hat{T}_t = \frac{1}{q}\sum_{i=-k}^{k} y_{t+1}, \tag{5}$$

where $q = 2k + 1$ is the order of the moving average. In other words, the estimate of the trend at time t is obtained by averaging values of the time series within k periods of t. The difference between the raw ACF and their moving average in Fig. 1 highlights the impact of flexibility in the force fields. As the stress tensor components are calculated at each time step, the presence of additional degrees of freedom in the flexible models produces additional perturbation in the averaged ACF, delaying equilibrium and, therefore, convergence of the ACF curves.

To further elucidate this, we plot, in Fig. 2, a comparison between the rigid force field's ACFs and the moving

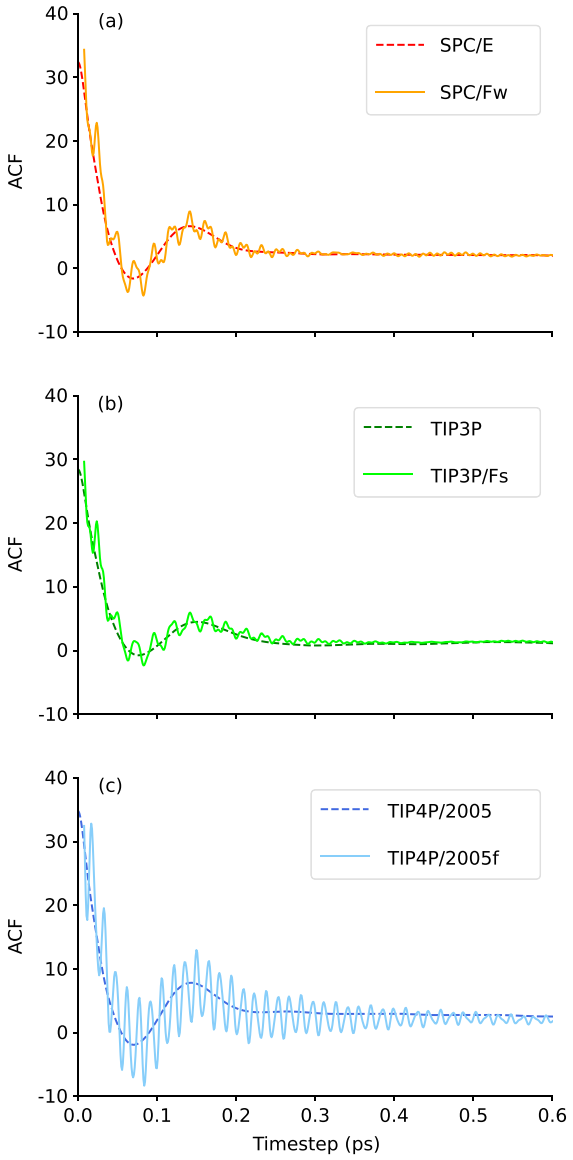

FIG. 2. Comparison between the rigid force field's ACF and the moving average for the flexible force field's ACF.

average of their respective flexible counterparts. We found that the moving average for a flexible force field's ACF fits perfectly with the rigid force field's ACF. The conclusion is that the white noise associated with the additional degrees of freedom in the flexible models is a direct consequence of the coupling between the harmonic perturbation introduced in the flexible force field and the reduced time interval used to calculate the stress tensor components. This is similar to the perturbation introduced by the carbon-oxygen interaction in a previous work, where repulsive LJ terms lead to difficult convergence in the ACF calculation of higher-density water-filled nanotubes [9].

In Fig. 3, we show the shear viscosity calculated for each model at different nanotube lengths l_z. We also plot the CI bars as a function of three independent simulations for each sample. Smaller values of viscosity were obtained for the TIP3P, both rigid and flexible, for all nanotube lengths. This trend follows the results obtained for bulk water (see Fig. S1 of the Supplemental Material [22]) and is in accordance with the work of González and Abascal [23], where rigid TIP4P viscosity estimations were bigger than those for TIP3P. On the other hand, the rigid TIP4P/2005 produced larger viscosity estimations, again in accordance with the bulk trend. In fact, while the difference between the rigid and flexible counterparts of the three-point force fields is small and lies within the CI bars, we found a larger difference for the four-point force fields (TIP4P/2005 and TIP4P/2005f). This difference is large enough to overcome the CI estimation and increases as the nanotube length decreases.

It means that the estimation of the viscosity of confined water is very sensitive to the families of force fields used in the simulations. This is a conclusion that can also be drawn by looking at the standard deviations for η in Tables S3 and S4 of the Supplemental Material [22]. It shows that the standard deviation of the shear viscosity among different water models simulated at the same CNT lengths is higher than the deviation of the same force-field models at different CNT lengths.

B. Water diffusion

To better understand the impact of the investigated models on the transport of water in carbon nanotubes, we also analyzed the diffusion coefficient. The diffusion coefficient is computed from the MSD of the water molecules' center of mass.

In Fig. 4, we present the MSD as a function of simulation time for the different water models confined in 40-nm-long CNTs. Following the trend of low viscosity, the TIP3P family presents the higher mobility among the force fields tested here. This is a behavior shared with simulations of bulk water shown in Fig. S1 of the Supplemental Material [22], and in accordance with recent theoretical works [10], showing that TIP3P self-diffusion is overestimated compared to experimental results.

From Fig. 5 and the data in Table S5 of the Supplemental Material [22], we can notice that, on average, the CI bars tend to decrease as we increase l_z. This is a direct consequence of the collective nature of the MSD and how it is calculated. For longer nanotubes, more particles contribute to the displacement computation and, by taking the mean value, we increase precision. However, we can see that the difference in CI estimates of between 80 and 160 nm is almost negligible, indicating that the length of the nanotube is no longer affecting the accuracy of diffusion computation. Here, we would like to mention the outstanding confidence estimate associated with the flexible SPC/Fw, which highlights their ability to capture the diffusion of water inside CNTs. Christofferson *et al.* [10] showed that for bulk systems, the diffusion coefficient calculated by this same model obtained a small percentage error of 12% compared to the experimental value. For both bulk and confined systems, the SPC/Fw model possesses the greatest precision. Tables S7 and S8 of the Supplemental Material [22] show the interference of force-field parameters in the self-diffusion coefficient calculation since the standard deviation among values obtained from different water models at the same CNT length is higher than those from the same models at different CNT lengths.

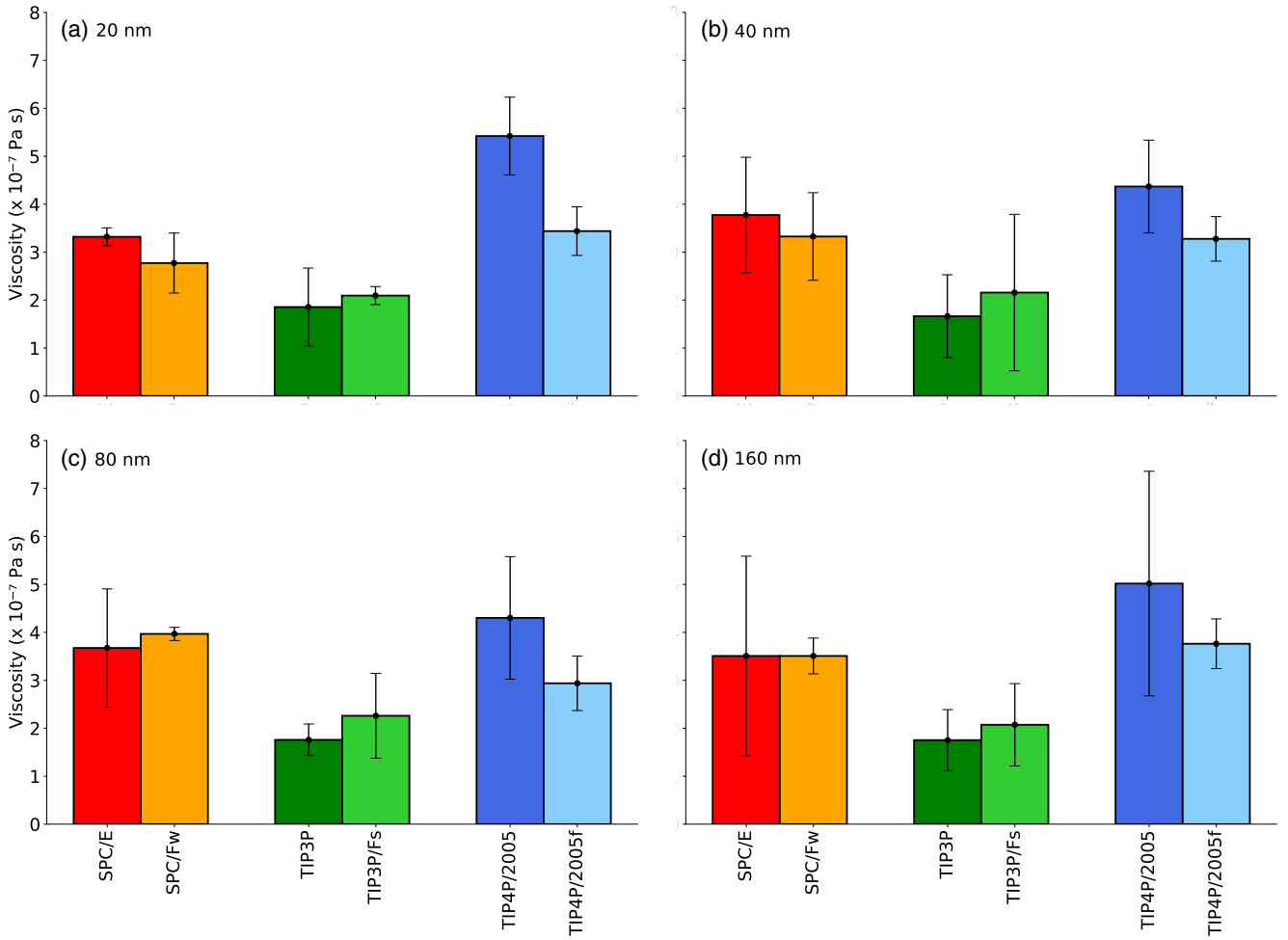

FIG. 3. Shear viscosity values for each rigid and flexible force field at nanotube lengths of (a) 20, (b) 40, (c) 80, and (d) 160 nm. The bars show the CI estimation.

Notably, the calculation of both transport coefficients (diffusion and viscosity) in an MD routine depends on many parameters and variables. For instance, Krishnan *et al.* [24] showed that the selection of thermostats has a considerable influence on the dynamic and structural properties of fluid molecules confined in small nanochannels. In Fig. S2 of the Supplemental Material [22], we show the impact of thermostatting on the dynamic properties studied here. We found higher values for viscosity (and lower diffusion) using the Langevin [25] thermostat in comparison to the Nosé-Hoover and Berendsen [26]. We observed the same trend whether we used the rigid SPC/E or the flexible SPC/Fw. This is consistent with results by Basconi and Shirts [27] for bulk water systems. In fact, Langevin thermostatting introduces friction and noise terms that can impact ACFs and dynamical properties. This can be observed in a study involving protein dynamics, where microcanonical dynamic features were not preserved using Langevin dynamics [28]. On the other hand, there are systems in which the Langevin dynamics provide a reliable temperature description, such as in catalytic heterogeneous interfaces [29]. The difference can be attributed to the way the thermostats control temperature and represents a very important aspect in MD simulations.

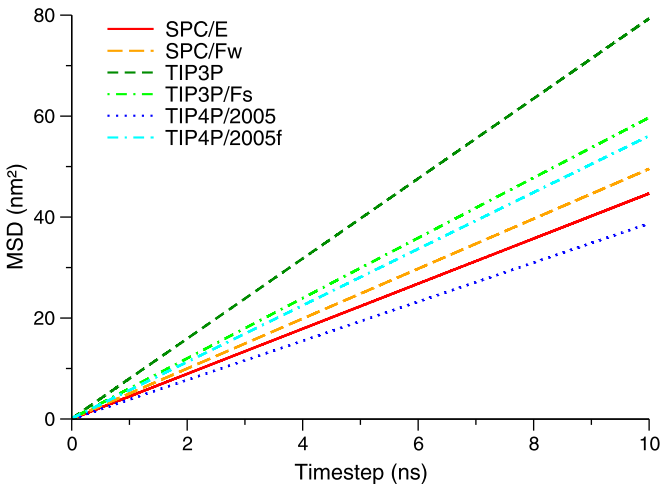

FIG. 4. The mean-squared displacement for the different rigid and flexible water models inside 40-nm-long CNTs.

As an additional parameter, we also performed a parametric study with shorter 1- and 5-nm-long (16,16) CNTs and the SPC force-field family. Figure S3 of the Supplemental Material [22] shows that while viscosity is not significantly affected, the diffusion of the flexible SPC/Fw increases as the

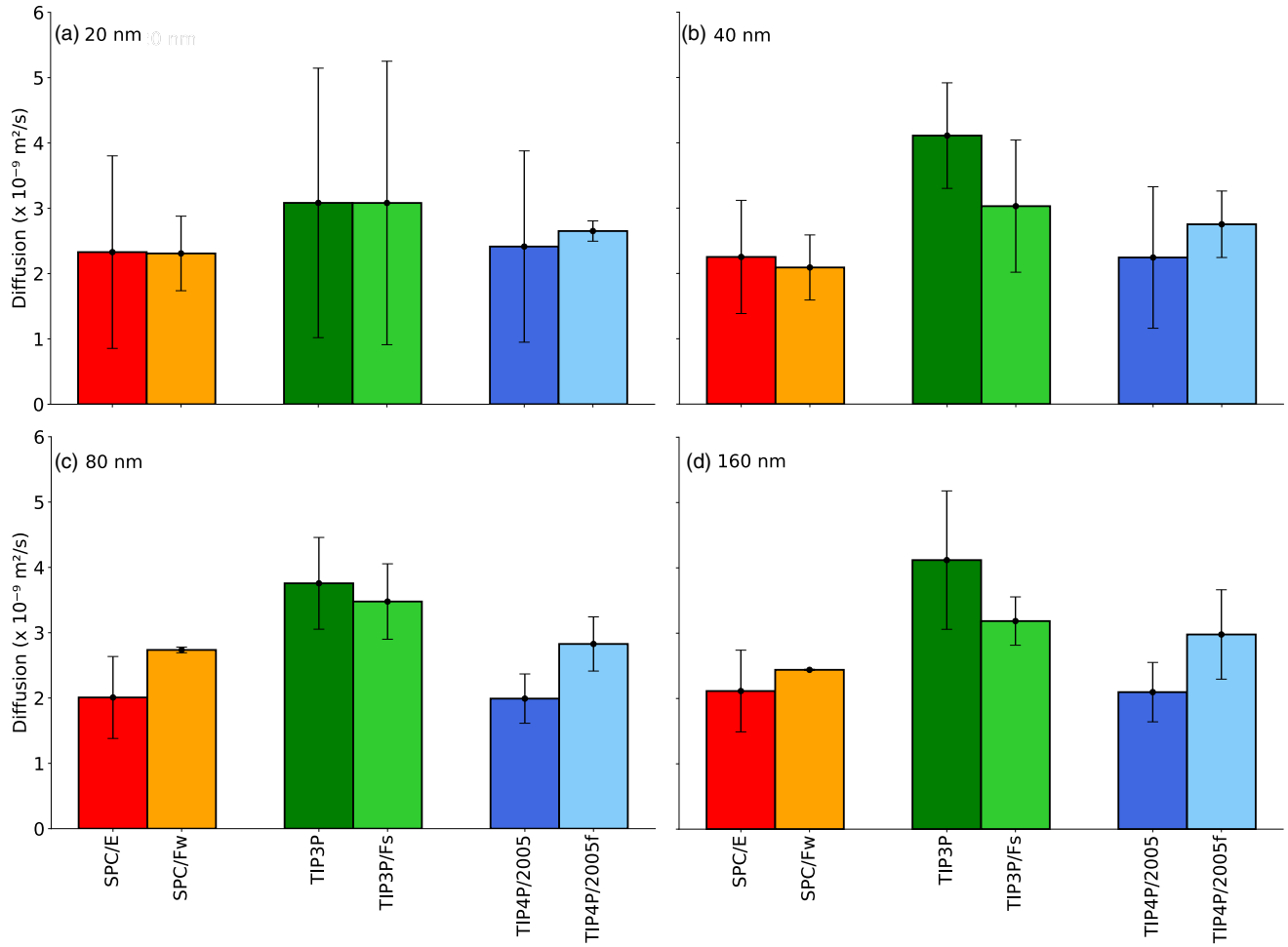

FIG. 5. Diffusion coefficient for each rigid and flexible force field at nanotube lengths of (a) 20, (b) 40, (c) 80, and (d) 160 nm. The bars show the CI estimation.

length of the nanotube becomes as small as 1 nm. Although the periodicity of the system in the axial direction implies an infinitely long nanotube, in a short unit cell (such as the 1 nm), the additional degrees of freedom of SPC/Fw would interfere with the thermal and dynamic correlations. It shows that a careful choice of the unit cell is crucial for an accurate analysis of the dynamical properties in these systems.

C. The radius factor

The dynamics of water confined in nanotubes is known to be a property highly affected by geometric parameters. For instance, Farimani and Aluru [8] found a dependence of the axial water diffusion on the radius r of the nanotube. Our group also found a mathematical expression for the dependence of the viscosity on the same variable [30]. In this section, we explore the variation of the dynamical and structural properties of water inside armchair nanotubes with different radii. We use (n, n) CNTs with $n = 10$, 12, 16, and 30, each of them containing 1000, 1600, 4500, and 14 500 water molecules, respectively, distributed along a length $l_z = 40$ nm.

In Fig. 6, we present the variation of both the viscosity and diffusion as a function of the nanotube radius, represented by different chiralities, for all the force fields. The three-point force fields (SPC and TIP3P families) show similar results (within the CI bars) for diffusion and viscosity when compared to their flexible counterparts. The four-point TIP4P/2005 and TIP4P/2005f also show good agreement in the viscosity for all the chiralities [Fig. 6(f)]. However, we found small differences in Fig. 6(c) regarding the diffusion estimation for (12,12) and (30,30) nanotubes, $r = 0.81$ and 2.03 nm, respectively. This can be a consequence of the narrow CI intervals found for these models, but also demonstrates the peculiarities of introducing additional degrees of freedom, such as flexibility. Markedly, all the force fields predict a rise in the diffusion (followed by a decrease in the viscosity) for (30,30) CNTs, in accordance with previous simulations with different water models [8,20].

One parameter affecting the dynamics of the confined water is the dipole alignment [31]. Here, we further investigate the alignment of the water dipole moment vector with the CNT axial direction, as represented in Fig. 7(a).

Figures 7(b)–7(g) show the dipole alignment for different force fields inside (10,10), (12,12), (16,16), and (30,30) CNTs. Most of the water models show alignment peaks around 40° and 140° inside the smaller (10,10) nanotube, while the flexible TIP3P/Fs exhibits only one sharp peak at

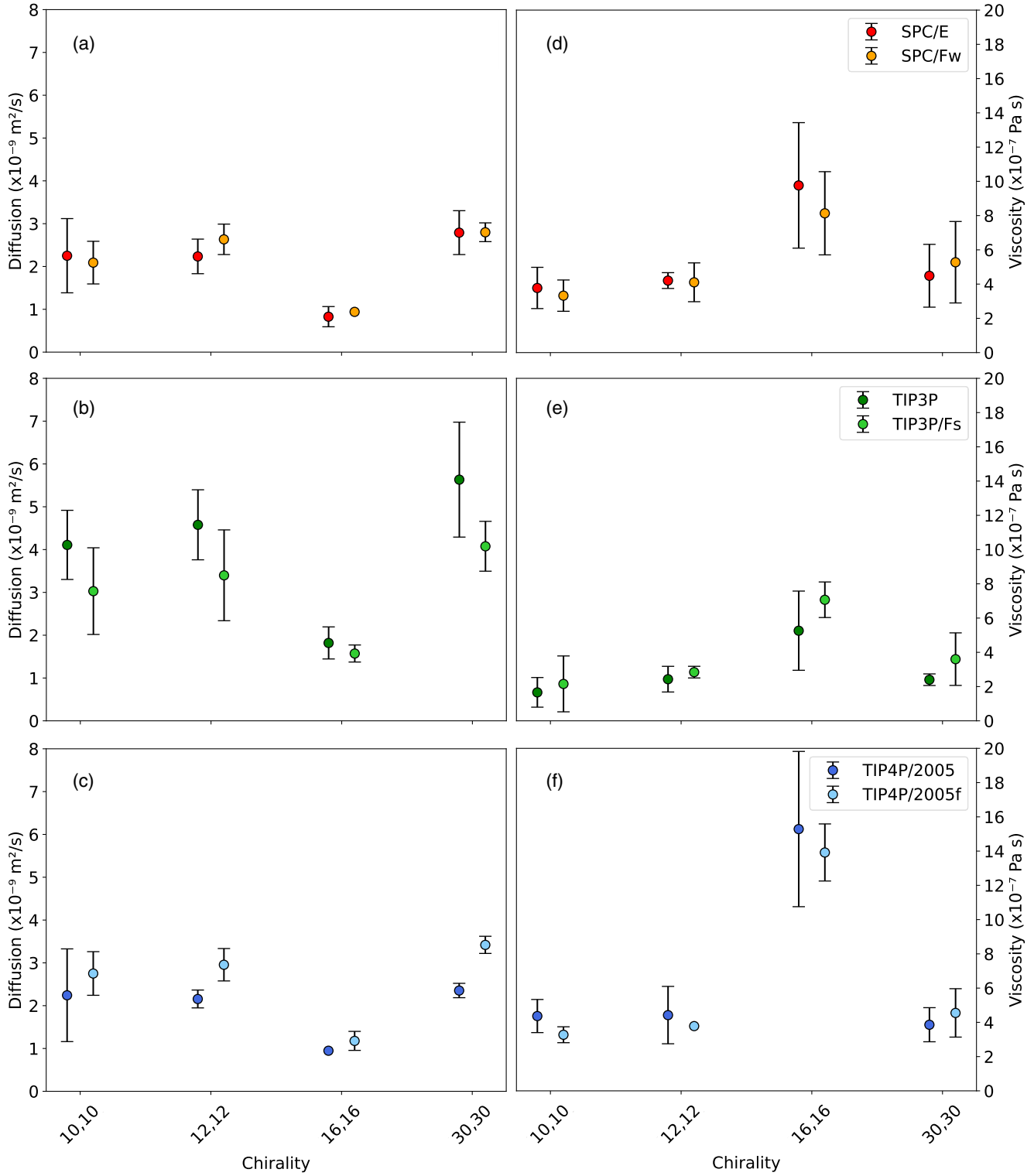

FIG. 6. Diffusion (left panel) and viscosity estimations (right panel) for different nanotube radii (chiralities) and force fields. CI bars are shown whenever they are bigger than the dots.

150°. It indicates a strong influence of this force field over the electrostatic properties of confined water. As the diameter is increased, the average dipole projection angle distribution becomes random for all force fields, suggesting that the dipole alignment is a consequence of the confinement level. Interestingly, Hemant *et al.* [32] showed that equilibrium simulations with the TIP3P water model produced angle distribution peaks at the same values found in this paper. It demonstrates that this is an intrinsic characteristic of the force field. From Fig. 7, we also found a negligible difference between rigid SPC/E

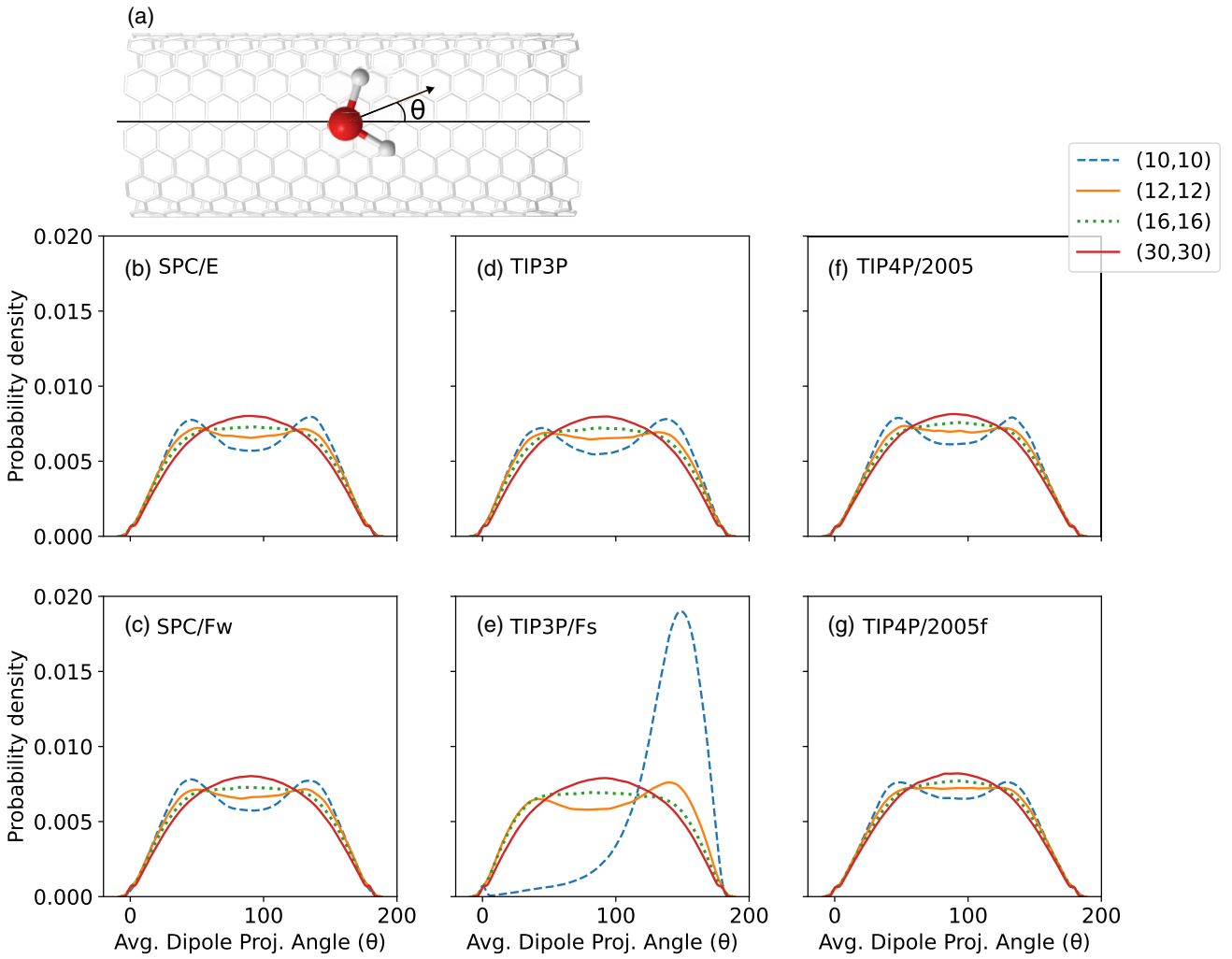

FIG. 7. Probability distribution of the dipole projection angle for (a) SPC/E, (b) SPC/Fw, (c) TIP3P, (d) TIP3P/Fs, (e) TIP4P/2005, and (f) TIP4P/2005f water models. Different color lines represent different CNT chiralities.

and its flexible counterpart SPC/Fw and between TIP4P/2005 and TIP4P/2005f for all nanotube sizes, so the response of each force field to the introduction of flexibility is different. Additionally, in a recent contribution, Liu *et al.* [33] found that components of the water dipole moment inside narrow nanotubes can be very different from each other, highlighting the directional nature of water molecules inside CNTs.

To better comprehend the dipole alignment of the confined TIP3P/Fs force field, we divide the inner region of the nanotube into two regions, i.e., one at the middle and the other at the water-wall interface, as shown in Figs. 8(i)–8(l). We also show, in Figs. 8(e)–8(h), the average density color map of the confined water.

We can see from Fig. 8(a) that the dipole orientation of TIP3P/Fs inside the smaller (10,10) nanotube is extremely directional. Both of the dipole alignments in regions 1 and 2 coincide with a sharp peak around 140°. Interestingly, as we increase the nanotube diameter, the alignment becomes dependent on the region the water molecule is in: two peaks (at 40° and 140°) are seen at the outer water layer in Figs. 8(b)–8(d) and a broad (more random) distribution is observed at the center of the nanotube. In Fig. S4 of the Supplemental Material [22], we see that the difference between the two regions is also observed for the rigid TIP3P model. However, instead of a single preferential dipole orientation observed for TIP3P/Fs, the rigid TIP3P inside the smaller (10,10) nanotube reproduces the same behavior as for the other chiralities, with two peaks at the water-wall interface and a broad Gaussian-like band at the middle of the nanotube. This difference between regions tells us that the water-wall interaction strongly affects the electrostatic properties of water models, and this effect is dependent on the size of the nanotube.

The structure assumed by water molecules inside the CNT is less susceptible to the flexibility introduced in the water model. Comparing the radial density color maps of Figs. 8(e)–8(h) and those in Fig. S4 of the Supplemental Material [22], we can notice that the structuration of water molecules is very similar: a single file enclosed by a tubelike interfacial structure in the smaller (10,10) CNT and, as the diameter is increased, a bulklike inner region and a dense-packed outer layer of water inside the (30,30) nanotube, as found elsewhere

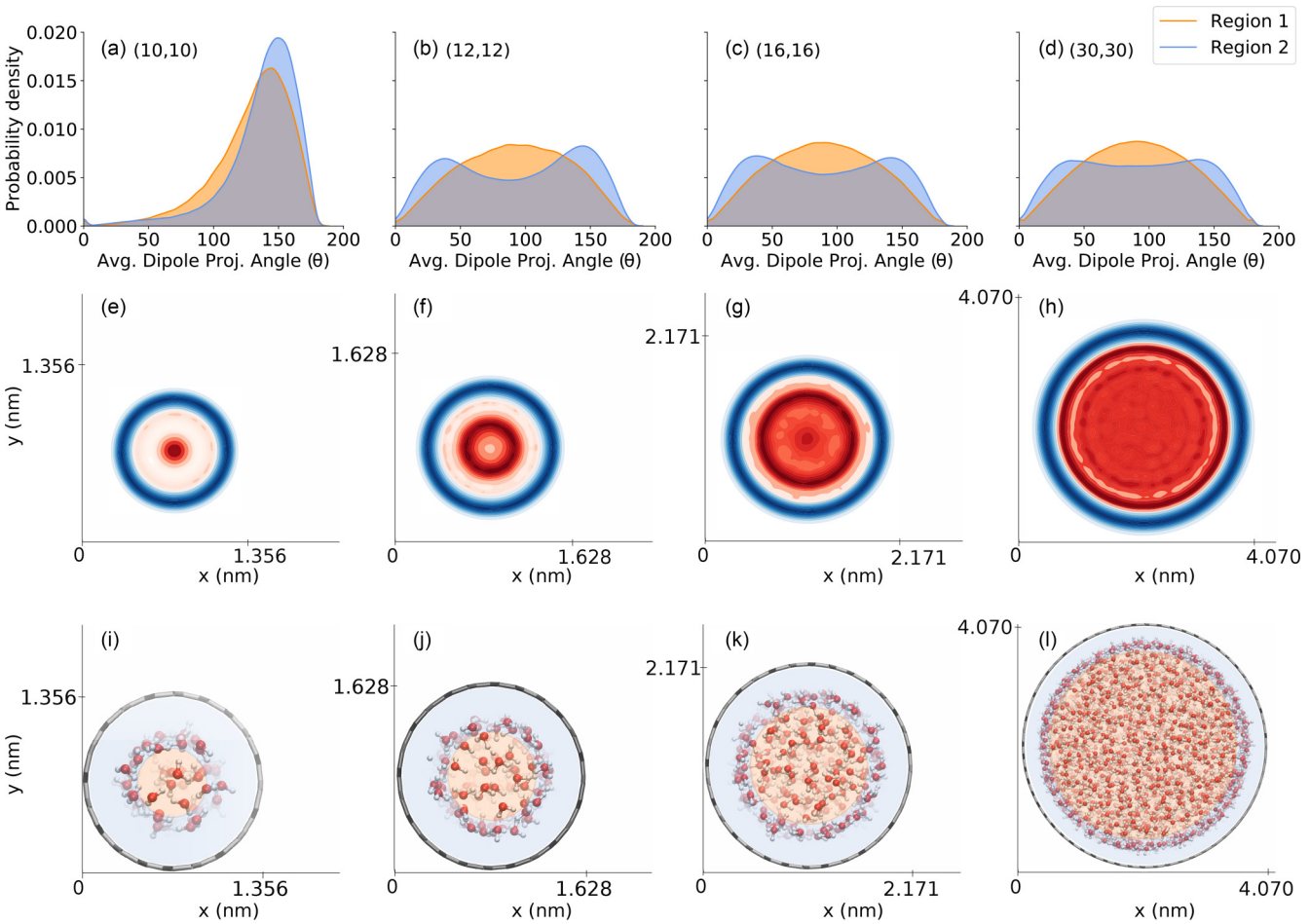

FIG. 8. Probability distribution of the dipole projection angle simulated with the TIP3P/Fs model divided in regions 1 and 2 for (a) (10,10), (b) (12,12), (c) (16,16), and (d) (20,20) nanotubes. In (e)–(h), we show the respective density color maps, and in (i)–(l), frontal snapshots of the final configurations, with schematic depictions of how we divided regions 1 and 2.

[30,34]. Therefore, the difference in the dipole alignment between force fields is restricted to electrostatic effects due to the charge distribution in each one of them. In Fig. S5 of the Supplemental Material [22], we also show the radial density plot for all the force fields to confirm that all of them exhibit very similar structuration.

D. Conclusions

In summary, we investigated the impact of force-field flexibility over dynamical and orientational aspects of water confined in CNTs. Among the six investigated water models, we found the flexible SPC/Fw to exhibit the smaller CI for both diffusion and viscosity.

We showed that the introduction of additional degrees of freedom leads to higher oscillations in the ACF of flexible water models. On the other hand, by taking their moving average, we can resume the ACF as in the rigid models. The viscosity calculation is, in turn, highly dependent on the force-field family, with lower values for the TIP3P family and higher values for rigid TIP4P/2005, as in the case of bulk water. This trend is also observed in the diffusion calculation, where the TIP3P family exhibits the higher mobility (although with the higher CI among all the models).

We found the dipole orientation along the nanotube to be extremely influenced by the force field. As an example of this, the flexible TIP3P/Fs showed a strong directionality inside the smaller (10,10) nanotube, with a sharp dipole alignment at 140°. We showed that the confinement level indeed affects water electrostatic and structural properties, with each force field featuring a different behavior as the diameter of the nanotube is decreased. We also found that the alignment of water at the interface is different from the alignment at the middle of the nanotube.

Finally, we showed flexibility to affect the dynamic estimation of confined three-point and four-point nonpolarizable models. Other degrees of freedom, such as additional charge points [35] or polarizability [36], and new methods such as density functional theory (DFT)- and machine learning-based force fields [10], are in continuous development. Recently, reactive potentials have also been tested for bulk water [37] and hydration of carbonate structures [38], with possible applications in the study of nanoconfined water. They will further help establish new information and fundamental aspects of nanofluidics and membrane science.

ACKNOWLEDGMENTS

The authors thank the Brazilian National Council for Scientific and Technological Development (CNPq), PQ Grant No. 306709/2021-0, and Research Support Foundation of the State of Rio Grande do Sul (FAPERGS), PqG Grant No. 21/2551-0002023-7, for funding support. This work used computational resources from CENAPAD-SP and CPAD-UFSM.

[1] M. H. Köhler, J. R. Bordin, C. F. de Matos, and M. C. Barbosa, Water in nanotubes: The surface effect, Chem. Eng. Sci. **203**, 54 (2019).

[2] M. W. Maddox and K. E. Gubbins, Molecular simulation of fluid adsorption in buckytubes, Langmuir **11**, 3988 (1995).

[3] G. Hummer, J. C. Rasaiah, and J. P. Noworytra, Water conduction through the hydrophobic channel of a carbon nanotube, Nature (London) **414**, 188 (2001).

[4] N. Naguib, H. Ye, Y. Gogotsi, A. G. Yazicioglu, C. M. Megaridis, and M. Yoshimura, Observation of water confined in nanometer channels of closed carbon nanotubes, Nano Lett. **4**, 2237 (2004).

[5] E. Secchi, S. Marbach, A. Nigues, D. Stein, A. Siria, and L. Bocquet, Massive radius-dependent flow slippage in carbon nanotubes, Nature (London) **537**, 210 (2016).

[6] J. Hassan, G. Diamantopoulos, L. Gkoura, M. Karagianni, S. Alhassan, S. V. Kumar, M. S. Katsiotis, T. Karagiannis, M. Fardis, N. Panopoulos, H. J. Kim, M. Beazi-Katsioti, and G. Papavassiliou, Ultrafast stratified diffusion of water inside carbon nanotubes; Direct experimental evidence with 2D $D - T_2$ NMR spectroscopy, J. Phys. Chem. C **122**, 10600 (2018).

[7] S. K. Kannam, B. D. Todd, J. S. Hansen, and P. J. Daivis, How fast does water flow in carbon nanotubes? J. Chem. Phys. **138**, 094701 (2013).

[8] A. B. Farimani and N. R. Aluru, Spatial diffusion of water in carbon nanotubes: From Fickian to ballistic motion, J. Phys. Chem. B **115**, 12145 (2011).

[9] M. H. Köhler, J. R. Bordin, L. B. da Silva, and M. C. Barbosa, Breakdown of the Stokes-Einstein water transport through narrow hydrophobic nanotubes, Phys. Chem. Chem. Phys. **19**, 12921 (2017).

[10] S. P. Pathirannahalage, N. Meftahi, A. Elbourne, A. C. G. Weiss, C. F. McConville, A. Padua, D. A. Winkler, M. Costa Gomes, T. L. Greaves, T. C. Le, Q. A. Besford, and A. J. Christofferson, Systematic comparison of the structural and dynamic properties of commonly used water models for molecular dynamics simulations, J. Chem. Inf. Model. **61**, 4521 (2021).

[11] A. P. Thompson, H. M. Aktulga, R. Berger, D. S. Bolintineanu, W. M. Brown, P. S. Crozier, P. J. Veld, A. Kohlmeyer, S. G. Moore, T. D. Nguyen, R. Shan, M. J. Stevens, J. Tranchida, C. Trott, and S. J. Plimpton, Lammps–A flexible simulation tool for particle-based materials modeling at the atomic, meso, and continuum scales, Comput. Phys. Commun. **271**, 108171 (2022).

[12] J.-P. Ryckaert, G. Ciccotti, and H. J. Berendsen, Numerical integration of the Cartesian equations of motion of a system with constraints: Molecular dynamics of n-alkanes, J. Comput. Phys. **23**, 327 (1977).

[13] H. J. C. Berendsen, J. R. Grigera, and T. P. Straatsma, The missing term in effective pair potentials, J. Phys. Chem. **91**, 6269 (1987).

[14] Y. Wu, H. L. Tepper, and G. A. Voth, Flexible simple point-charge water model with improved liquid-state properties, J. Chem. Phys. **124**, 024503 (2006).

[15] W. L. Jorgensen, J. Chandrasekhar, J. D. Madura, R. W. Impey, and M. L. Klein, Comparison of simple potential functions for simulating liquid water, J. Chem. Phys. **79**, 926 (1983).

[16] U. W. Schmitt and G. A. Voth, The computer simulation of proton transport in water, J. Chem. Phys. **111**, 9361 (1999).

[17] J. L. F. Abascal and C. Vega, A general purpose model for the condensed phases of water: TIP4P/2005, J. Chem. Phys. **123**, 234505 (2005).

[18] M. A. González and J. L. F. Abascal, A flexible model for water based on TIP4P/2005, J. Chem. Phys. **135**, 224516 (2011).

[19] S. Nosé, A molecular dynamics method for simulations in the canonical ensemble, Mol. Phys. **52**, 255 (1984).

[20] Y.-G. Zheng, H.-F. Ye, Z.-Q. Zhang, and H.-W. Zhang, Water diffusion inside carbon nanotubes: Mutual effects of surface and confinement, Phys. Chem. Chem. Phys. **14**, 964 (2012).

[21] M. P. Allen and D. J. Tildesley, *Computer Simulation of Liquids* (Oxford University Press, Oxford, 1989), p. 408.

[22] See Supplemental Material at http://link.aps.org/supplemental/10.1103/PhysRevE.108.034116 for details of the viscosity and diffusion confidence intervals and standard deviations, results for bulk water, different thermostats, and dipole alignment for the rigid TIP3P model.

[23] M. Gonzalez and J. Abascal, The shear viscosity of rigid water models, J. Chem. Phys. **132**, 096101 (2010).

[24] T. V. S. Krishnan, J. S. Babu, and S. P. Sathian, A molecular dynamics study on the effect of thermostat selection on the physical behavior of water molecules inside single walled carbon nanotubes, J. Mol. Liq. **188**, 42 (2013).

[25] T. Schneider and E. Stoll, Molecular-dynamics study of a three-dimensional one-component model for distortive phase transitions, Phys. Rev. B **17**, 1302 (1978).

[26] H. J. C. Berendsen, J. P. M. Postma, W. F. van Gunsteren, A. DiNola, and J. R. Haak, Molecular dynamics with coupling to an external bath, J. Chem. Phys. **81**, 3684 (1984).

[27] J. E. Basconi and M. R. Shirts, Effects of temperature control algorithms on transport properties and kinetics in molecular dynamics simulations, J. Chem. Theory Comput. **9**, 2887 (2013).

[28] D. J. Tobias, G. J. Martyna, and M. L. Klein, Molecular dynamics simulations of a protein in the canonical ensemble, J. Phys. Chem. **97**, 12959 (1993).

[29] V. Korpelin, T. Kiljunen, M. M. Melander, M. A. Caro, H. H. Kristoffersen, N. Mammen, V. Apaja, and K. Honkala, Addressing dynamics at catalytic heterogeneous interfaces with DFT-MD: Anomalous temperature distributions from commonly used thermostats, J. Phys. Chem. Lett. **13**, 2644 (2022).

[30] M. H. Köhler and L. B. da Silva, Size effects and the role of density on the viscosity of water confined in carbon nanotubes, Chem. Phys. Lett. **645**, 38 (2016).

[31] D. N. de Freitas, B. H. Mendonca, M. H. Köhler, M. C. Barbosa, M. S. Matos, R. C. Batista, and A. B. de Oliveira, Water diffusion in carbon nanotubes under directional electric fields: Coupling between mobility and hydrogen bonding, Chem. Phys. **537**, 110849 (2020).

[32] H. Kumar, S. Bera, S. Dasgupta, A. K. Sood, C. Dasgupta, and P. K. Maiti, Dipole alignment of water molecules flowing through a carbon nanotube, Phys. Rev. B **107**, 165402 (2023).

[33] D. Liu, J. Li, J. Wu, and D. Lu, *Ab initio* molecular dynamics simulation of water transport through short carbon nanotubes, ACS Omega **7**, 40466 (2022).

[34] M. H. Köhler, J. R. Bordin, L. B. da Silva, and M. C. Barbosa, Structure and dynamics of water inside hydrophobic and hydrophilic nanotubes, Physica A **490**, 331 (2018).

[35] C.-L. Zhao, D.-X. Zhao, C.-C. Bei, X.-N. Meng, S. Li, and Z.-Z. Yang, Seven-site effective pair potential for simulating liquid water, J. Phys. Chem. B **123**, 4594 (2019).

[36] I. Leven, H. Hao, A. K. Das, and T. Head-Gordon, A reactive force field with coarse-grained electrons for liquid water, J. Phys. Chem. Lett. **11**, 9240 (2020).

[37] O. R. Gittus and F. Bresme, Thermophysical properties of water using reactive force fields, J. Chem. Phys. **155**, 114501 (2021).

[38] K. Palczynski, T. Kirschbaum, A. Bande, and J. Dzubiella, Hydration structure of diamondoids from reactive force fields, J. Phys. Chem. C **127**, 3217 (2023).